






Controlling entanglement in a triple-well system of dipolar atoms

K. Wittmann W. ^{1,*}, L. H. Ymai ², B. H. C. Barros ¹, J. Links ³ and A. Foerster ^{1,†}

¹*Instituto de Física da UFRGS, Porto Alegre, RS 91501-970, Brazil*

²*Universidade Federal do Pampa, Bagé, RS 96413-170, Brazil*

³*School of Mathematics and Physics, The University of Queensland, Brisbane 4072, Australia*



(Received 30 May 2023; accepted 6 September 2023; published 21 September 2023)

We study the dynamics of entanglement and atomic populations of ultracold dipolar bosons in an aligned three-well potential described by an extended Bose-Hubbard model. We focus on a sufficiently strong interacting regime where the couplings are tuned to obtain an integrable system, in which the time evolution exhibits a resonant behavior that can be exactly predicted. Within this framework, we propose a protocol that includes an integrability breaking step by tilting the edge wells for a short time through an external field, allowing the production of quantum states with a controllable degree of entanglement. We analyze this protocol for different initial states and show the formation of highly entangled states as well as NOON-like states. These results offer valuable insights into how entanglement can be controlled in ultracold atom systems that may be useful for the proposals of new quantum devices.

DOI: [10.1103/PhysRevA.108.033313](https://doi.org/10.1103/PhysRevA.108.033313)

I. INTRODUCTION

Quantum entanglement is a phenomenon discovered in the foundations of quantum physics that paved the way for a new era of technological advances. It represents nonlocal correlations between separate parts of a quantum system. As a resource, entanglement has been proven to be very useful for performing numerous tasks that face barriers in a classical setting, finding broad applications in quantum information processing [1–6], quantum teleportation [7–11], quantum secure communication [12,13], and quantum metrology and sensing [14–16].

Entangled states are key ingredients in the proposals of protocols for the development of new quantum devices [17–23], and hence understanding the mechanisms for producing and controlling entangled states with a high degree of precision is of fundamental importance. In this context, the search for highly entangled states is the aim of many technological quantum applications [24], which can be exploited through different platforms. Among these, ultracold atoms are especially interesting because current techniques enable the manipulation of atoms arranged in optical potentials, with astonishing precision and versatility of the operating control [25–27].

In recent experiments on ultracold quantum gases, dipolar bosons are loaded into optical lattices to generate long-range dipole-dipole interaction (DDI), allowing access to fascinating quantum properties and phases [28]. The dynamics of such dipolar boson systems have been intensively studied and described, with good results, by an extended Bose-Hubbard model (EBHM) [29,30]. One interesting feature of the EBHM with few bosonic modes is that the couplings of interactions can be tuned to achieve an integrable regime, which

is particularly suited for the design of quantum devices. For instance, in Ref. [31], the conserved charge provided by integrability plays a crucial role when examining the quantum dynamics of a dipolar Bose-Einstein condensate (BEC) on a three-well aligned system, making it a potential candidate for constructing an atomic transistor [32]. Other integrable quantum systems are being recently utilized to support the development of quantum technologies. These include quantum circuits created from transfer matrices [33] and those created through the star-triangle relation [34], central spin models for quantum sensors [35], and the preparation of Bethe states on a quantum computer [36–39].

Here we consider an integrable triple-well model of dipolar bosons and propose a protocol to create quantum states with controllable entanglement level. The control is realized by breaking the integrability for a short time and the resulting entanglement is characterized by the von Neumann entropy and correlation functions. We test the protocol for a range of different initial states, demonstrating how to produce highly entangled states as well as other important quantum states such as NOON-like states [40].

The paper is organized as follows. In Sec. II, we describe the system and discuss the conditions for obtaining an effective description of the integrable system in the resonant regime. In Sec. III, we analyze the dynamics of the system and the entanglement behavior in the resonant regime. In Sec. IV, we propose a protocol for controlling entanglement by briefly tilting the edge sites of the system. In Secs. V–VII, we analyze the action of the protocol on different initial states. A discussion on interferometric applications of the protocol and details on the ground state structure are provided in the Appendices. The conclusions are given in Sec. VIII.

II. SYSTEM DESCRIPTION

We consider a system of dipolar atoms in an aligned triple-well potential described by the following extended

*karinwittmannwilsmann@gmail.com

†angela@if.ufrgs.br

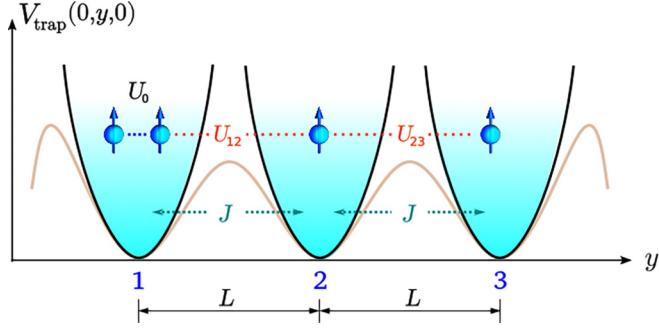


FIG. 1. Schematic representation of the triple-well system. Dipolar atoms are confined by the potential trap V_{trap} with the wells aligned along the y axis. The neighboring wells are separated by a distance L . The arrows represent the dipoles of atoms oriented along the direction of polarization (assumed to be in the z direction). The coupling J represents the hopping rate, U_0 characterizes on-site interactions, while U_{ij} characterizes the DDI between particles on different sites.

Bose-Hubbard model:

$$H = \frac{U_0}{2} \sum_{i=1}^3 N_i(N_i - 1) + \sum_{i=1}^3 \sum_{j=1; j \neq i}^3 \frac{U_{ij}}{2} N_i N_j - \frac{J}{\sqrt{2}} (a_1^\dagger a_2 + a_2^\dagger a_1 + a_2^\dagger a_3 + a_3^\dagger a_2), \quad (1)$$

where a_i , a_i^\dagger , and $N_i = a_i^\dagger a_i$ are the bosonic annihilation, creation, and number operators of the well (or site) $i = 1, 2, 3$, respectively. The coupling J denotes the hopping rate of atoms between neighboring wells and U_0 and $U_{ij} = U_{ji}$ set the on-site and long-range interactions, respectively. The on-site interaction $U_0 = U_{sr} + U_{dd}$ results from short range interaction U_{sr} and on-site dipole-dipole interaction (DDI) U_{dd} . The short-range interaction $U_{sr} \propto 4\pi \hbar^2 a/m$ is determined by the s -wave scattering length a , which is controlled through a magnetic field via Feshbach resonance, and m is the mass of the atom. The on-site DDI $U_{dd} \propto \mu^2$ and long-range interactions $U_{ij} \propto \mu^2$ follow from an inverse cubic law of the relative position between polarized particles whose strength is determined by the permanent magnetic dipole moment μ of dipolar atoms considered, and highly depends on the geometry of potential trap and the polarization direction of dipoles [29,41]. A schematic representation of this system is presented in Fig. 1.

For potential wells aligned along the y axis, separated by a distance L at the same depth, and with all dipoles oriented in the z direction, the interaction energies are balanced, satisfying $U_{12} = U_{23}$ as a consequence of symmetry. After setting the value of the s -wave scattering length, the depth of the wells can be tuned to satisfy the condition $U_{13} = U_0$ (see Appendix A). Under these conditions, the Hamiltonian given by Eq. (1) is integrable [42] and can be reduced, up to a global constant, to

$$H = U(N_1 - N_2 + N_3)^2 - \frac{J}{\sqrt{2}} (a_1^\dagger a_2 + a_2^\dagger a_1 + a_2^\dagger a_3 + a_3^\dagger a_2), \quad (2)$$

where $N = N_1 + N_2 + N_3$ is the total number of particles and $U = (U_0 - U_{12})/4$ represents the effective interaction energy. A discussion on the feasibility of a physical realization of this system by means of Bose-Einstein condensates of dipolar atoms can be found in Ref. [31]. In this integrable case, the model can be formulated and solved using the quantum inverse scattering method and Bethe ansatz methods [42]. The system acquires the additional conserved operator

$$Q = \frac{1}{2}(N_1 + N_3 - a_1^\dagger a_3 - a_3^\dagger a_1), \quad (3)$$

besides the Hamiltonian H and the total number of particles N , resulting in three independent conserved operators in an equal number of system modes. The conserved charge Q plays an important role in the *resonant regime*, characterized by the emergence of coherent oscillations of the atomic populations in the edge wells (labeled by $i = 1$ and 3), with atoms passing directly through the middle well ($i = 2$) without accumulating in it as a consequence of a second-order process that occurs in a relatively strong interaction regime [29,43]. This behavior can be understood from the combination of two opposite effects. On the one hand, in the relatively strong interaction regime, the identification of single mode $a_{13} \equiv (a_1 + a_3)/\sqrt{2}$ of sites 1 and 3 provides the two-site structure of the Hamiltonian (see Appendix B) that leads to a self-trapping behavior [44] and, consequently, to the conservation of atomic population initially in the subsystem of wells 1 and 3. On the other hand, the condition of integrability cancels the interaction energy $(U_{13} - U_0)N_1 N_3$ in the Hamiltonian so that sites 1 and 3 effectively form a noninteracting double-well system, with the atomic population free to oscillate harmonically within this subsystem [see Fig. 2(a)]. In order to reach the resonant regime we consider the initial state

$$|\Psi_0\rangle = |N - k - l, l, k\rangle, \quad (4)$$

where l ($l = 0, \dots, N$) and k ($k = 0, \dots, N - l$) represent the number of atoms initially at wells 2 and 3, respectively. The resonant regime is then achieved when $|U(N - 2l)/J| \gg 1$ and the quantum dynamics of the Hamiltonian (2) can be well described by the effective Hamiltonian [31],

$$H_{\text{eff}} = \omega_l Q, \quad (5)$$

where constant ω_l is given by

$$\omega_l = \lambda_l J^2, \quad (6)$$

with $\lambda_l = \frac{1}{4|U|} (\frac{l+1}{N-2l-1} - \frac{l}{N-2l+1})$ depending on the initial number l of bosons in the middle well. The constant ω_l will play the role of the resonant tunneling frequency, with period $T_l = 2\pi/\omega_l$. For the case where $l = 0$, let us simply denote it by $T \equiv T_0$.

In the following sections, we first discuss the dynamical quantities that characterize the behavior of the system and provide information about its quantum entanglement. After that, we provide a protocol that briefly tilts wells 1 and 3 to control the entanglement of the quantum state. Then, we analyze the effects of the protocol on different initial states.

III. DYNAMICS OF POPULATIONS AND ENTANGLEMENT

We start by considering the dynamics of the system described above in the integrable and resonant regime, and for

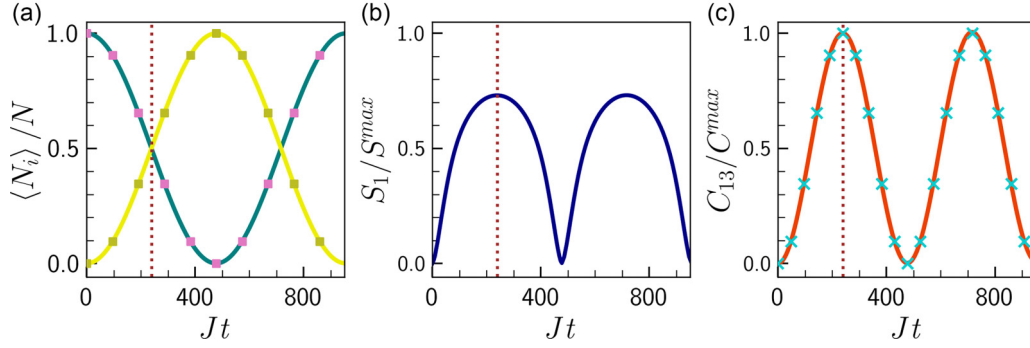


FIG. 2. (a) Fractional expectation values $\langle N_i \rangle / N$ (green line) and $\langle N_3 \rangle / N$ (yellow line) for $N = 20$, initial state $|\Psi_0\rangle = |20, 0, 0\rangle$, $U = -2$, and $J = 1$. The marks represent the analytic expression (10). (b) Time evolution of the entanglement entropy S_1 in units of $S_1^{\max} = \ln(N + 1)$. (c) Time evolution of correlation functions C_{13} in units of $C_{13}^{\max} = N/4$. The numerical simulation (11) is represented by the solid line, while the marks result from the closed form expression. The vertical dotted lines mark the instant $t = T/4$, where $\langle N_1 \rangle = \langle N_3 \rangle$ and the values of S_1 and C_{13} are maximum.

convenience, we set $\hbar = 1$. We focus on the time evolution of the average number of particles per well

$$\langle N_i \rangle = \langle \Psi(t) | N_i | \Psi(t) \rangle \quad (7)$$

and the von Neumann entanglement entropy

$$S_i(t) = -\text{Tr}[\rho_i(t) \ln \rho_i(t)], \quad (8)$$

where the density matrix is defined as $\rho(t) = |\Psi(t)\rangle\langle\Psi(t)|$ and $\rho_i(t)$ is the reduced density matrix of site i where the remaining subsystem is traced out. The von Neumann entropy quantifies the bipartite entanglement between the site i and the subsystem of the other two sites. In the integrable regime, an initial state described by $|\Psi_0\rangle$ will evolve in time according to

$$|\Psi(t)\rangle = \mathcal{U}(t)|\Psi_0\rangle, \quad (9)$$

where $\mathcal{U}(t) \equiv e^{-iHt}$ is the time-evolution operator. In what follows, we will use $|\Psi\rangle$ to refer to states obtained using the Hamiltonian (2), and we will use the notation $|\tilde{\Psi}\rangle$ with a tilde to denote analytic states obtained using the effective Hamiltonian (5), from which analytic results can be derived. A comparison between the quantum states $|\Psi\rangle$ and $|\tilde{\Psi}\rangle$ obtained for the same set of parameters will be quantified through the fidelity defined as $F = |\langle\Psi|\tilde{\Psi}\rangle|^2$. We will consider that the state $|\Psi\rangle$ theoretically approaches the analytic state $|\tilde{\Psi}\rangle$ when $F > 0.95$.

For the case of initial state (4), the state $|\tilde{\Psi}(t)\rangle$ predicts that $\langle N_2 \rangle = l$ remains constant, while the atoms oscillate harmonically between sites $i = 1$ and $i = 3$, according to the expectation values given by [31]

$$\langle N_i \rangle = \frac{1}{2}[N - l + (2 - i)(N - l - 2k) \cos(\omega t)]. \quad (10)$$

The expression above shows a maximum amplitude with oscillations of period $T = 2\pi/\omega_0$ when all atoms are initially located in one of the edge wells (i.e., when $|\Psi_0\rangle = |N, 0, 0\rangle$ or $|\Psi_0\rangle = |0, 0, N\rangle$) and an equilibrium with $\langle N_1 \rangle = \langle N_3 \rangle = N/2$ remaining constant when the edge wells initially have the same number of atoms (i.e., when $|\Psi_0\rangle = |n, 0, n\rangle$, with $N = 2n$). These two extreme cases will be the subject of our study later on. In Fig. 2 are shown some numerical results for the case $|\Psi_0\rangle = |N, 0, 0\rangle$ using the Hamiltonian (2). Figure 2(a)

shows the perfect agreement between the results of the numerical simulation and the expectation values given in (10). In Fig. 2(b) the time evolution of the entanglement entropy S_1 presents a period of $T/2$ and its first maximum occurring at $t = T/4$, exactly when the populations reach an equilibrium with $\langle N_1 \rangle = \langle N_3 \rangle$. Nevertheless, despite the fact that the von Neumann entanglement entropy is the most frequently used measure to quantify entanglement, it does not depend on any particular observable, making it difficult to perform a direct experimental measurement of its magnitude. In order to generate signatures to indicate the formation of highly entangled states, in addition to enabling experimental measurements, we also evaluate the two-site correlation function defined as

$$C_{ij} \equiv |\langle N_i \rangle \langle N_j \rangle - \langle N_i N_j \rangle|. \quad (11)$$

Using the state $|\tilde{\Psi}(t)\rangle$, we can derive the correlation function in the closed form $C_{13} = (N/4) \sin^2(t \omega_0)$, from which a maximum value is directly obtained at $t = T/4$. The agreement between numerical simulation of C_{13} and its analytic formula can be seen in Fig. 2(c). From Figs. 2(b) and 2(c) it is clear that the maximum values of the two-site correlation functions and the entanglement entropy occur simultaneously. This result shows that the two-site correlation function is also able to reveal information about the quantum entanglement of the subsystem of wells.

It is worth noting that the entanglement entropy S_2 vanishes, since the state of site 2 remains constant in the resonant regime, while $S_1 = S_3 \neq 0$ shows that bipartite entanglement is present only in the subsystem of sites 1 and 3.

IV. PROTOCOL FOR QUANTUM ENTANGLEMENT CONTROL

We now focus on establishing a protocol for generating and controlling maximally entangled states. The control of quantum entanglement can be achieved by tilting wells 1 and 3 through the action of an additional coherent light beam superimposed on the triple-well system designed on an optical trap. During the presence of tilt on wells 1 and 3 the dynamics is

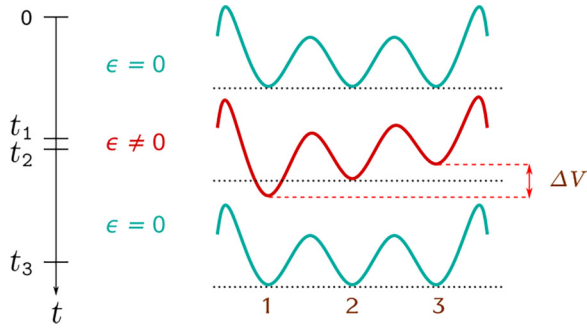


FIG. 3. Schematic representation of the control protocol sequence. The tilt ΔV between the potentials of sites 1 and 3 is induced through an external field. The duration of the field allows the entanglement in the subsystem consisting of sites 1 and 3 to be controlled.

governed by the Hamiltonian [32]

$$\mathcal{H}(\epsilon) = H + \epsilon(N_3 - N_1), \quad (12)$$

where H is the integrable Hamiltonian (2) and the parameter ϵ characterizes the energy offset between edge potential wells (see Fig. 3). Other properties of this Hamiltonian (12) can be found in Refs. [31,45,46]. Here we will examine the case where the tilt is introduced into the protocol as a short-duration square pulse just after the initial state evolves to the state with maximum correlation at $t = T/4$, as identified in the previous section. It will be seen that the amount of quantum entanglement is completely determined by the duration of the square pulse.

The full description of the protocol can be represented as follows:

$$|\Psi(t)\rangle = |\Psi_k(t)\rangle, \quad t_{k-1} \leq t \leq t_k,$$

where the states for steps $k = 1, 2$, and 3 of the protocol are given sequentially by

$$|\Psi_1(t)\rangle = \mathcal{U}(t - t_0, 0)|\Psi_0\rangle,$$

$$|\Psi_2(t)\rangle = \mathcal{U}(t - t_1, \epsilon)|\Psi_1(t_1)\rangle,$$

$$|\Psi_3(t)\rangle = \mathcal{U}(t - t_2, 0)|\Psi_2(t_2)\rangle.$$

Here, $\mathcal{U}(t, \epsilon) \equiv e^{-i\mathcal{H}(\epsilon)t}$ is the time evolution operator. This sequence is depicted in Fig. 3 below, illustrating the dependence on the parameter ϵ .

In what follows, we continue to adopt the notation $|\Psi\rangle$ (without tilde) for states obtained using the Hamiltonian (12), and $|\tilde{\Psi}\rangle$ for analytic states obtained using the effective Hamiltonian $\mathcal{H}_{\text{eff}}(\epsilon) = H_{\text{eff}} + \epsilon(N_3 - N_1)$, where H_{eff} is given by (5).

At the end of the whole process, the protocol generates the state

$$\begin{aligned} |\Psi_{\text{out}}\rangle &\equiv |\Psi_3(t_3)\rangle \\ &= \mathcal{U}(\Delta t_3, 0)\mathcal{U}(\Delta t_2, \epsilon)\mathcal{U}(\Delta t_1, 0)|\Psi_0\rangle, \end{aligned} \quad (13)$$

where $\Delta t_k = t_k - t_{k-1}$ is the duration of the k th ($k = 1, 2, 3$) step of the protocol. As mentioned earlier, we are assuming that $t_0 = 0$, $\Delta t_1 = T/4$, and $\Delta t_2 \ll \Delta t_{1,3}$ such that the breaking of integrability is the dominant effect in the second step of the protocol. In the following sections, the action of the protocol on different initial input states will be investigated in detail.

V. FOCK INPUT STATE

We start by first considering the case of a completely localized initial state given by $|\Psi_0\rangle = |N, 0, 0\rangle$. Figure 4 shows the effect of the protocol on the dynamics for different values

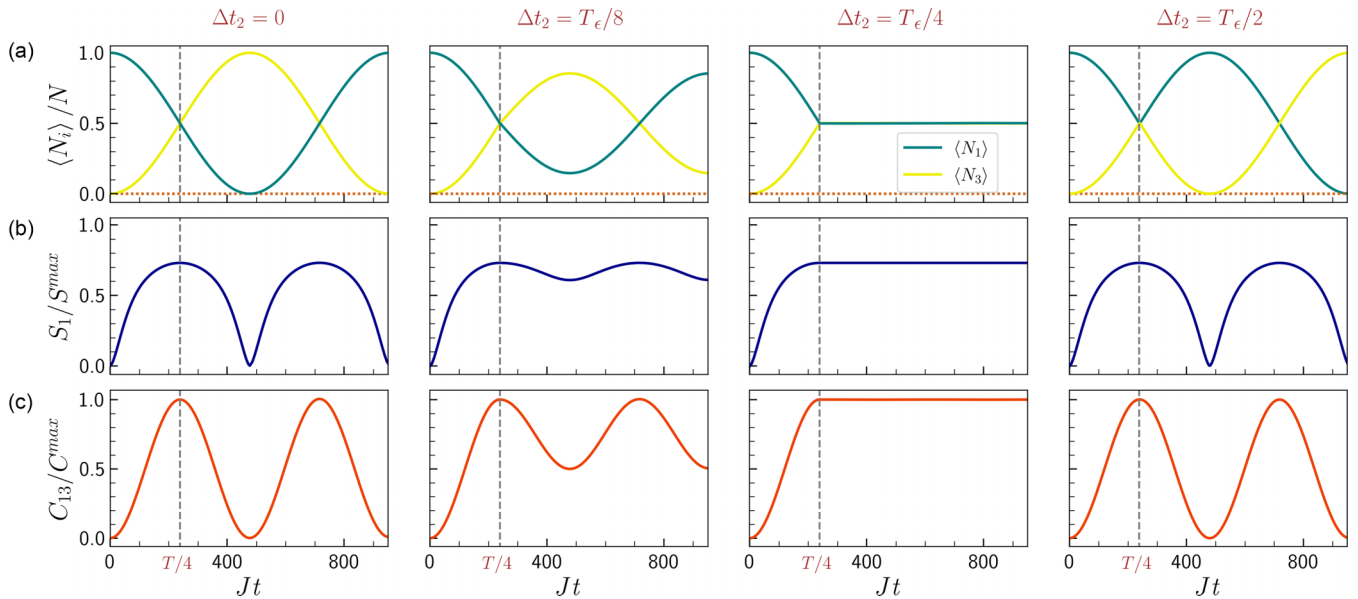


FIG. 4. Time evolution of the fractional expectation values (row a) $\langle N_1 \rangle / N$ (green line), $\langle N_2 \rangle / N$ (dotted line), $\langle N_3 \rangle / N$ (yellow line); entanglement entropy in units of $S_1^{\text{max}} = \ln(N + 1)$ (row b); and two-site correlation function in units of $C_{13}^{\text{max}} = N/4$ (row c). Each column represents a different value of Δt_2 . The first column represents the integrable case, where $\Delta t_2 = 0$. The other columns show the cases where $\Delta t_2 = T_\epsilon/8$, $\Delta t_2 = T_\epsilon/4$, and $\Delta t_2 = T_\epsilon/2$, in sequence. In all cases, $N = 20$, initial state $|\Psi_0\rangle = |20, 0, 0\rangle$, $U = -2$, $J = 1$, and $\epsilon = 1$. The vertical dashed lines represent the instant $t = t_2$.

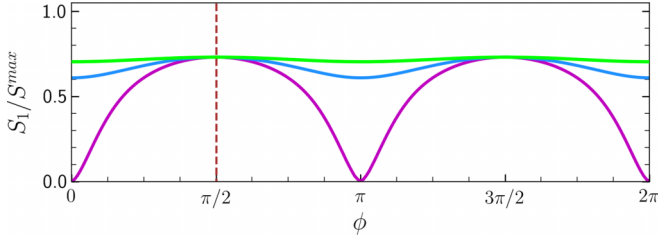


FIG. 5. Entanglement entropy of state $|\Psi_{\text{out}}\rangle$ as function of $\phi \in [0, 2\pi]$ for $\Delta t_3 = T/16$ (green), $\Delta t_3 = T/8$ (blue), and $\Delta t_3 = T/4$ (magenta), for $N = 20$, using the initial state $|\Psi_0\rangle = |20, 0, 0\rangle$, $U = -2$, $J = 1$, and $\epsilon = 1$. The dashed vertical line represents $\Delta t_2 = T_\epsilon/4$.

of duration of a square pulse Δt_2 counted in units of period $T_\epsilon = 2\pi/\Omega_\epsilon$, where $\Omega_\epsilon = 2\epsilon$.

In the first line of the Fig. 4, after the action of the square pulse ($t \geq t_2$), the expectation value of the fractional population of sites $i = 1, 3$ is shown, which is given by

$$\langle N_i \rangle / N = 1/2 - (1 - i/2) \sin[\omega_0(t - t_2)] \cos \phi, \quad (14)$$

and ϕ is a dimensionless parameter defined as

$$\phi = 2\epsilon \Delta t_2.$$

We observe that the amplitude of the expectation values of $\langle N_i \rangle / N$ decreases gradually with increasing the pulse duration Δt_2 until the dynamics becomes stationary balanced for a long time at $\Delta t_2 = T_\epsilon/4$ (or $\phi = \pi/2$) and completely reversed at $\Delta t_2 = T_\epsilon/2$ (or $\phi = \pi$). In the second line of Fig. 4, the range of values of entanglement entropy gradually decreases with increasing duration of the pulse, becoming stationary at its maximum value at $\Delta t_2 = T_\epsilon/4$. The dynamics of entanglement of the state $|\Psi(t)\rangle$ along the control process is also signaled in the third line of Fig. 4 through the correlation function of sites 1 and 3.

In Fig. 5 we present the entanglement entropy of state $|\Psi_{\text{out}}\rangle$ as a function of ϕ for three time intervals $\Delta t_3 = T/16, T/8, T/4$. We observe that entanglement entropy can be controlled over a larger range of values at $\Delta t_3 = T/4$. Therefore, for fixed duration $\Delta t_3 = T/4$, the protocol predicts the following quantum state:

$$|\tilde{\Psi}_{\text{out}}(\phi)\rangle = \frac{[\sin(\phi/2)a_1^\dagger + \cos(\phi/2)a_3^\dagger]^N}{\sqrt{N!}}|0, 0, 0\rangle, \quad (15)$$

where $|0, 0, 0\rangle$ is the vacuum state. From the above expression, the correlation function of sites 1 and 3 can be determined analytically as a function of parameter ϕ and it is given by $C_{13} = (N/4) \sin^2 \phi$. When performing the control within the interval $\Delta t_2 \in [0, T_\epsilon]$, the expression above shows that the maximized correlation $C_{13}^{\text{max}} = N/4$ occurs at $\phi = \pi/2 (3\pi/2)$, when the state $|\Psi_{\text{out}}\rangle$ has the maximum entanglement entropy with all atoms into the (anti)symmetric coherent state with fidelity $F = 0.99827 (0.999509)$:

$$|\tilde{\Psi}_{\text{out}}\rangle = \frac{(a_1^\dagger \pm a_3^\dagger)^N}{\sqrt{2^N N!}}|0, 0, 0\rangle.$$

If all atoms are initially loaded into site 3 (i.e., $|\Psi_0\rangle = |0, 0, N\rangle$), the states with maximum correlation are generated

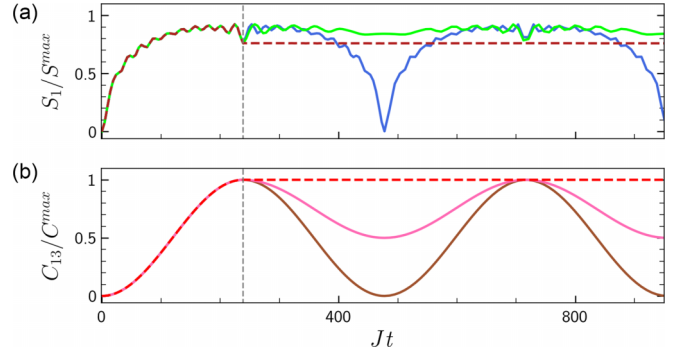


FIG. 6. (a) Entanglement entropy for $\Delta t_2 = 0$ (blue line), $\Delta t_2 = T_\epsilon/8$ (green line), and $\Delta t_2 = T_\epsilon/4$ (dashed line), and (b) correlation for $\Delta t_2 = 0$ (brown line), $\Delta t_2 = T_\epsilon/8$ (pink line), and $\Delta t_2 = T_\epsilon/4$ (dashed line). For all cases, the initial state $|\Psi_0\rangle = |10, 0, 10\rangle$ was used for $N = 20$, $U = -2$, $J = 1$, and $\epsilon = 1$. The vertical dashed lines represent the instant $t = t_2$.

with symmetry reversed compared to the case where $|\Psi_0\rangle = |N, 0, 0\rangle$. In the next section, we consider the case where initially both sites 1 and 3 have the same number of atoms.

VI. TWIN-FOCK INPUT STATE

In this section we investigate the quantum entanglement control for the case of the initial twin-Fock state in sites 1 and 3, given by $|\Psi_0\rangle = |n, 0, n\rangle$, for which $N = 2n$ and the expectation values $\langle N_1 \rangle = \langle N_3 \rangle = n$ remain constant under integrable time evolution in the resonant regime. Figure 6 presents the dynamics of the entanglement entropy of state $|\Psi(t)\rangle$ for three different durations of a square pulse.

Again, for $\Delta t_2 = T_\epsilon/4$, the entanglement entropy is stationary.

Figure 7 shows the entanglement entropy S_1 as a function of dimensionless parameter ϕ and three time intervals $\Delta t_3 = T/16, T/8$, and $T/4$. In this case, the output state $|\Psi_{\text{out}}\rangle$ presents high entanglement entropy with a small dip at $\Delta t_2 = T_\epsilon/4$ in its signature, and for $\Delta t_3 = T/4$ the state predicted by our protocol is given by

$$|\tilde{\Psi}_{\text{out}}(\phi)\rangle = \frac{(2 \cos \phi a_1^\dagger a_3^\dagger + \sin \phi [(a_1^\dagger)^2 - (a_3^\dagger)^2])^n}{2^n n!} |0, 0, 0\rangle. \quad (16)$$

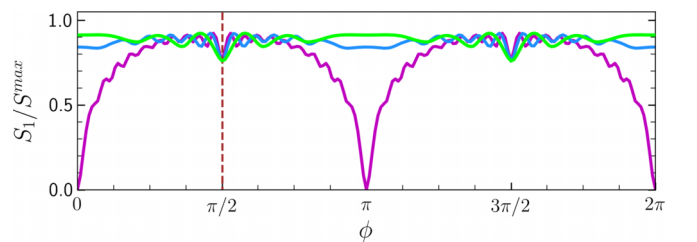


FIG. 7. Entanglement entropy of state $|\Psi_{\text{out}}\rangle$ as a function of $\phi \in [0, 2\pi]$ for $\Delta t_3 = T/4$ (magenta), $\Delta t_3 = T/8$ (blue), and $\Delta t_3 = T/16$ (green), using the initial state $|\Psi_0\rangle = |10, 0, 10\rangle$, for $N = 20$, $U = -2$, $J = 1$, $\epsilon = 1$, and $\Delta t_1 = T/4$. The dashed vertical line represents $\Delta t_2 = T_\epsilon/4$.

The above state allows determining analytically the correlation function of sites 1 and 3 as a function of parameter ϕ , given by

$$C_{13} = \frac{n(n+1)}{2} \sin^2 \phi.$$

In particular, for $\phi = \pi/2$ and $\phi = 3\pi/2$, the correlation achieves its maximum value $C_{13} = n(n+1)/2$ and the state $|\tilde{\Psi}_{\text{out}}\rangle$ is highly entangled with the respective fidelities $F = 0.998315$ and $F = 0.998771$, given by (up to global phase)

$$|\tilde{\Psi}_{\text{out}}\rangle = \frac{[(a_1^\dagger)^2 - (a_3^\dagger)^2]^n}{2^n n!} |0, 0, 0\rangle.$$

The above state shows that the protocol acts on the initial twin-Fock state by performing a discrete Fourier transform on modes 1 and 3 defined as $a_{1(3)}^\dagger \rightarrow (a_1^\dagger \pm a_3^\dagger)/\sqrt{2}$ [47], which leads to a quantum state with only an even number of particles at sites 1 and 3. This result can be interpreted as a destructive interference process on the odd number of particles, similar to the well-known Hong-Ou-Mandel (HOM) effect [48,49].

It is worth noting that, in the resonant regime, the time evolution operators $\mathcal{U}(T/4, 0)$ and $\mathcal{U}(\Delta t_2, \epsilon)$ used to generate the output state $|\Psi_{\text{out}}\rangle$ play an analogous role of the 50:50 beam-splitter and phase-shifter operations in a Mach-Zehnder (MZ) interferometer [50,51] This shows the protocol is capable of performing interferometric operations in which the phase estimation sensitivity depends on the choice of the initial state and the observable to be detected (see Appendix C).

VII. ENTANGLED INPUT STATE

In the previous sections, we considered a class of nonentangled initial states in which the state of well 2 remains constant over time, and therefore remains disentangled from the rest of the system. Now we will consider an entangled initial state in which quantum entanglement between well 2 and the subsystem composed of the other two wells is also manifest. To this end, let us analyze the effect of the protocol on the initial state defined as

$$|\Psi_0\rangle = \frac{1}{\sqrt{2}} |0, N, 0\rangle + \frac{1}{\sqrt{2N!}} \left(\frac{a_1^\dagger + a_3^\dagger}{\sqrt{2}} \right)^N |0, 0, 0\rangle. \quad (17)$$

The above state has a NOON-like state (NLS) structure, in the sense that it is a superposition between the state with all particles in well 2 and the state with all atoms in the subsystem of wells 1 and 3. However, the state of the subsystem of wells 1 and 3 has all particles into a coherent state $|\text{CS}\rangle = \frac{1}{\sqrt{N!}} \left(\frac{a_1^\dagger + a_3^\dagger}{\sqrt{2}} \right)^N |0, 0, 0\rangle$. The motivation for its study lies in the possibility of the three-well system to serve as a basic component for directing the transfer of two-mode NOON states within a larger integrated network. In addition, the NLS is directly related to the ground state of the integrable Hamiltonian (see Appendix B), which in principle could be prepared in the laboratory by controlling the system parameters.

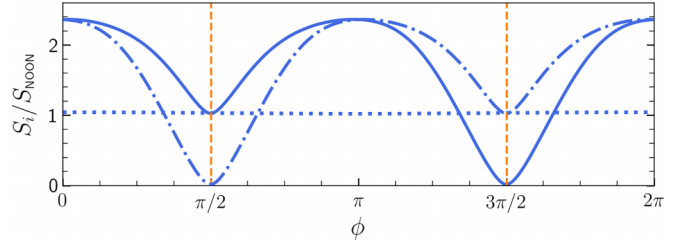


FIG. 8. Entanglement entropies (in units of $S_{\text{NOON}} = \ln 2$) S_1 (solid line), S_2 (dot line), and S_3 (dot-dashed line) of state $|\tilde{\Psi}_{\text{out}}\rangle$ (18) as a function of $\phi \in [0, 2\pi]$, for $N = 10$ and $U = -1.3$.

Now, considering the case of initial state (17), the effective Hamiltonian is still given by (5) with $l = 0$, since $\omega_N = \omega_0$. Then, the protocol predicts the following quantum state:

$$|\tilde{\Psi}_{\text{out}}(\phi)\rangle = \frac{1}{\sqrt{2}} |0, N, 0\rangle + \frac{1}{\sqrt{2N!}} (c_\phi a_1^\dagger - s_\phi a_3^\dagger)^N |0, 0, 0\rangle, \quad (18)$$

where we define

$$c_\phi = \cos\left(\frac{\phi}{2} - \frac{\pi}{4}\right), \quad s_\phi = \sin\left(\frac{\phi}{2} - \frac{\pi}{4}\right).$$

Figure 8 presents the change of entanglement entropies S_1 , S_2 , and S_3 with respect to the parameter ϕ . The figure clearly shows that the entropy S_2 remains constant at $S_2 = \ln 2$ while the other entropies exhibit a dip at $\phi = \pi/2(3\pi/2)$ with the typical value $S_{1(3)} = \ln 2$ of a NOON state.

In addition, the two-site correlation functions obtained from the quantum state (18) are given by (see Fig. 9)

$$\begin{aligned} C_{13} &= \frac{N(N-2)}{16} \cos^2 \phi, \\ C_{12} &= \frac{N^2}{4} \cos^2\left(\frac{\phi}{2} - \frac{\pi}{4}\right), \\ C_{23} &= \frac{N^2}{4} \sin^2\left(\frac{\phi}{2} - \frac{\pi}{4}\right). \end{aligned}$$

From Fig. 9, it is clear the occurrence of maximum of C_{12} coincides with the cancellation of C_{23} and vice versa when

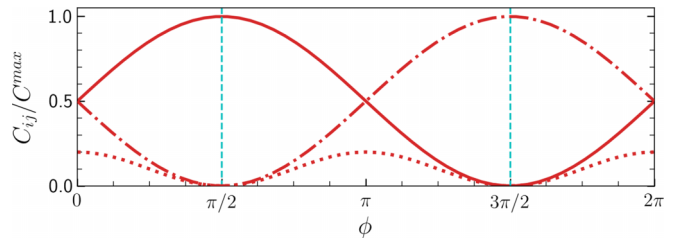


FIG. 9. Correlation functions (in units of $C^{\text{max}} = N^2/4$) C_{12} (solid line), C_{23} (dot-dashed line), and C_{13} (dot line) for $N = 10$ and $U = -1.3$.

$C_{13} = 0$, at $\phi = \pi/2$, and $\phi = 3\pi/2$, producing the corresponding states

$$\begin{aligned} |\tilde{\Psi}_{\text{out}}(\pi/2)\rangle &= \frac{1}{\sqrt{2}}|0, N, 0\rangle + \frac{1}{\sqrt{2}}|N, 0, 0\rangle, \\ |\tilde{\Psi}_{\text{out}}(3\pi/2)\rangle &= \frac{1}{\sqrt{2}}|0, N, 0\rangle + \frac{(-1)^N}{\sqrt{2}}|0, 0, N\rangle, \end{aligned}$$

with the fidelities $F = 0.996123$ and $F = 0.973085$, respectively. The above NOON states can be seen as the result of an entanglement deconcentration process [52–54] through unitary transformation on the NLS state, since they are produced in the subsystems 12 and 23 with less entanglement entropy $S_{1,3}$ than the initial state. This result shows that the protocol controls the transition between the biseparable and fully entangled quantum state of a tripartite system [55], since only two modes are entangled in the states $|\tilde{\Psi}_{\text{out}}(\pi/2)\rangle$ and $|\tilde{\Psi}_{\text{out}}(3\pi/2)\rangle$, whereas all modes are entangled in the states $|\Psi_{\text{out}}(0)\rangle$ or $|\Psi_{\text{out}}(\pi)\rangle$ [see Eq. (18)]. It also suggests that the triple-well system can be thought of as a potential shared router operating at the interface between two individual quantum devices to perform a transfer of a NOON state. The triple-well system itself can be viewed as an example of two interconnected double-well systems, where each of them can perform Mach-Zehnder interferometry using the NOON input state [56]. In addition, the three-well system can be appropriately integrated into a larger arrangement of wells where it and the subsystems in its vicinity can be individually confined and sequentially manipulated via additional external fields. This makes it possible to apply the functionality of the three-well system to more complex well network architectures.

VIII. CONCLUSION

We have proposed a protocol to generate states with controlled levels of entanglement, where the control is realized by breaking the integrability for a short period of time. Our study provides closed formulas for correlation functions to characterize the entanglement in terms of the integrability breaking time, which allowed us to predict the time required to generate highly entangled states. In the action of protocol on one of the initial states, the maximum correlation predicts the formation of NOON states, whereas, for other unentangled initial states, the maximum correlations are closely related to interference processes.

Our results have the potential to open new avenues for the manipulation and short-range transfer of entangled states within multimode systems. This can be achieved, for instance, by adapting the steps of our protocol to small parts of a multimode system through the application of external local fields. In future research, we will adjust our protocol to investigate the transfer of entangled states in the four-well system in ring and star configurations, which are the simplest geometries after the three-well model within the family of integrable multiwell systems [42]. These studies may find applications in quantum routing processes of new devices based on ultracold quantum technology.

ACKNOWLEDGMENTS

The authors acknowledge support from CNPq (Conselho Nacional de Desenvolvimento Científico e Tecnológico) - Edital Universal 406563/2021-7. A.F. and J.L. are supported by the Australian Research Council through Discovery Project No. DP200101339. We thank Rafael Barfknecht for helpful discussions. J.L. acknowledges the traditional owners of the land on which The University of Queensland (St. Lucia campus) operates, the Turrbal and Jagera people.

APPENDIX A: INTEGRABILITY CONDITION

In this section, we provide additional information on the integrability condition, aiming to offer a physical description of its experimental feasibility. To calculate the interaction parameters, we consider the wells to be aligned along the y direction, where the position of the center of site i is denoted by $\mathbf{r}_{i=1,2,3}$, and the neighboring sites are separated by a distance L . We assume that atoms are tightly confined in the optical trap and the interaction energies involved are not strong enough to excite higher Bloch bands, so that the wave function $W_i(\mathbf{r}) = W(\mathbf{r} - \mathbf{r}_i)$ of site i is a Gaussian of the form $W(\mathbf{r}) = \varphi(x)\varphi(y)\varphi(z)$, where

$$\varphi(b) = \left(\frac{1}{\pi\sigma_b^2}\right)^{1/4} e^{-b^2/(2\sigma_b^2)},$$

$\sigma_{b=x,y,z} = \sqrt{\hbar/(m\omega_b)}$ is the width of Gaussian, and $\omega_{b=x,y,z}$ denote the trap frequency in the b direction, which can be tuned by the potential depth of optical trap. The interaction parameters are given by [43]

$$\begin{aligned} U_{sr} &= \frac{4\pi\hbar^2 a}{m} \int |W_1|^4 d\mathbf{r}, \\ U_{ij} &= \int |W_i(\mathbf{r})|^2 |W_j(\mathbf{r}')|^2 V_{dd}(\mathbf{r} - \mathbf{r}') d\mathbf{r} d\mathbf{r}', \\ U_{dd} &= U_{11}, \end{aligned}$$

where m is the mass of the dipolar atom considered, the short-range interaction U_{sr} is controlled by s -wave scattering length a via Feshbach resonance, U_{dd} arises from the dipole-dipole interaction (DDI) between particles in the same site, while U_{ij} ($i \neq j$) refers to DDI between particles on different sites. The DDI is governed by the inverse cubic law of the distance $r = |\mathbf{r}|$ between two polarized dipoles, whose potential is defined by

$$V_{dd}(\mathbf{r}) = \frac{\mu_0\mu^2}{4\pi} \frac{(1 - 3\cos^2\theta)}{r^3},$$

where μ_0 is vacuum magnetic permeability, μ is the permanent magnetic dipole moment of the dipolar atom considered, and θ is the angle between the dipole polarization and the relative position $\mathbf{r} - \mathbf{r}'$. In addition, we are assuming that all dipoles are oriented along the z direction [see Fig. 10(a)].

For the case $\sigma \equiv \sigma_x = \sigma_y$ and $\sigma_z = \sigma/\kappa$, the aspect ratio κ determines the three possible geometries of a potential trap: prolate shape ($\kappa < 1$), spherical ($\kappa = 1$), or oblate shape ($\kappa > 1$) [57]. By setting the dimensionless parameters $q \equiv d/(\sqrt{2}\sigma)$ and $\beta \equiv a/a_{dd}$, where d is the distance between sites i and j and $a_{dd} = \mu_0\mu^2 m/(12\pi\hbar^2)$ is the dipolar length,

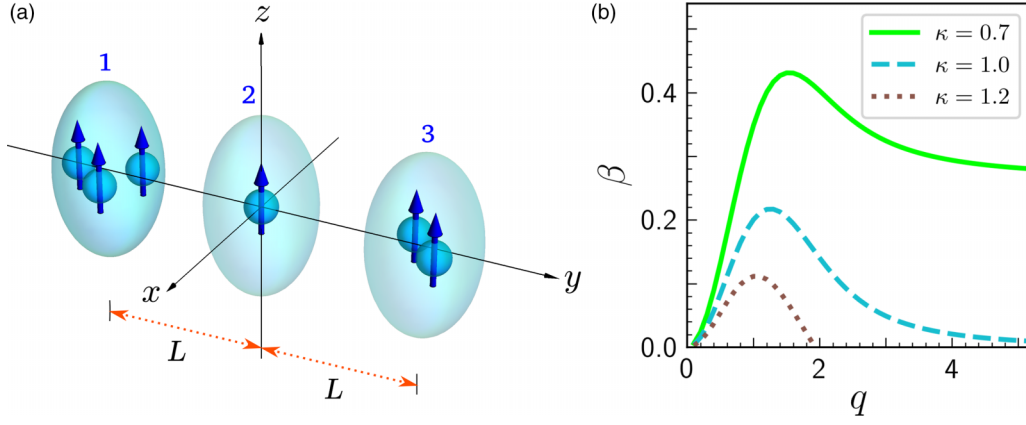


FIG. 10. (a) Schematic figure of the triple-well system. The wells are aligned along the y axis, with the neighboring wells separated by a distance L , and dipoles (represented by the arrows) are polarized along the z direction. (b) The parameter β as function of q for the aspect ratios $\kappa = 0.7$ (solid line), $\kappa = 1.0$ (dashed line), and $\kappa = 1.2$ (dotted line). It can be observed that the curves possess an absolute maximum value $\beta_{\max} = \max_q \beta(q)$ for which the interval of scattering length $0 < a \leq \beta_{\max} a_{dd}$ allows to obtain the integrability.

the interaction energy parameters can be calculated using the Fourier transform [29], resulting in the formulas

$$U_{sr} = \frac{4\pi\hbar^2 a \kappa}{m} \left(\frac{q}{d\sqrt{\pi}} \right)^3,$$

$$U_{dd} = -\beta^{-1} f(\kappa) U_{sr},$$

$$U_{ij} = 2\beta^{-1} U_{sr} \left[e^{-q^2} - \frac{3}{q^2} \int_0^q \frac{t^2(1-t^2)e^{-t^2}}{\sqrt{\kappa^2 q^2 + t^2(1-\kappa^2)}} dt \right],$$

where

$$f(\kappa) = \frac{1+2\kappa^2}{1-\kappa^2} - \frac{3\kappa^2 \operatorname{arctanh} \sqrt{1-\kappa^2}}{(1-\kappa^2)^{3/2}}$$

expresses that the nature of the on-site DDI is dependent on the geometry of the potential trap. In particular, $U_{dd} = 0$ for spherical trap potential, since $\lim_{\kappa \rightarrow 1} f(\kappa) = 0$. The condition of integrability $U_{ij} = U_0 = U_{sr} + U_{dd}$ allows to obtain the parameter β as function of q :

$$\beta(q) = f(\kappa) + 2e^{-q^2} - \frac{6}{q^2} \int_0^q \frac{t^2(1-t^2)e^{-t^2}}{\sqrt{\kappa^2 q^2 + t^2(1-\kappa^2)}} dt,$$

which provides the tolerances on the scattering length values needed to maintain integrability in an experiment, since the function $\beta(q)$ is clearly upper-bounded, as can be seen in Fig. 10(b). The above equation can be numerically solved to provide the trap frequencies

$$\omega_x = \omega_y = \frac{2\hbar}{m} \left(\frac{q}{d} \right)^2, \quad \omega_z = \kappa^2 \omega_x$$

that allow to achieve the integrable regime. For the integrability condition $U_{13} = U_0$, we consider $d = 2L$.

APPENDIX B: GROUND STATE

In this section, we discuss the structure of the ground state of integrable Hamiltonian (2) in the resonant regime with $U < 0$, with the aim of clarifying the conditions required to prepare the initial state used in Sec. VII. To this end, we

first note that the Hamiltonian (2) can be reduced to a Bose-Hubbard Hamiltonian of a two-site structure (see, for instance, Ref. [58])

$$H = U(N_{13} - N_2)^2 - J(a_2^\dagger a_{13} + a_{13}^\dagger a_2),$$

by identifying the single-mode operator $a_{13} = \frac{a_1 + a_3}{\sqrt{2}}$ and the total number of particles $N_{13} = N_1 + N_3$ in the subsystem of sites 1 and 3. On the other hand, for a small number of atoms, it is known that the ground state of the two-site Bose-Hubbard Hamiltonian admits the generation of NOON state $|\text{NOON}\rangle = \frac{1}{\sqrt{2}}(|N, 0\rangle + |0, N\rangle)$ in the strong repulsive interaction regime [59], which has the entanglement entropy $S_{\text{NOON}} = -\operatorname{Tr}(\rho_1 \ln \rho_1) = \ln 2$ due to it having only one pair of equally likely base Fock states. Likewise, in the resonant regime (with $U < 0$) for small $N \sim 10$, the ground state $|\text{GS}\rangle$ of the three-mode integrable Hamiltonian (2) presents high fidelity (above 0.99) to the NOON-like state (NLS),

$$|\text{NLS}\rangle = \frac{1}{\sqrt{2}}|0, N, 0\rangle + \frac{1}{\sqrt{2}} \frac{(a_{13}^\dagger)^N}{\sqrt{N!}}|0, 0, 0\rangle.$$

Figure 11 presents the fidelity $F = |\langle \text{NLS} | \text{GS} \rangle|^2$ as a function of $|U/J|$ and N for $U < 0$.

APPENDIX C: INTERFEROMETRY

In this section, we discuss some interferometric aspects of the protocol proposed in Sec. IV.

First, we consider the state produced in Eq. (15) to calculate the imbalance population between sites 1 and 3. This provides an interference pattern as a function of parameter ϕ according to the equation

$$\langle N_1 - N_3 \rangle \equiv \langle \tilde{\Psi}_{\text{out}}(\phi) | N_1 - N_3 | \tilde{\Psi}_{\text{out}}(\phi) \rangle = -N \cos \phi.$$

Note that the unconventional negative sign can be changed by extending the duration of the last operation to $\Delta t_3 = 3T/4$. The phase uncertainty can be obtained using the error

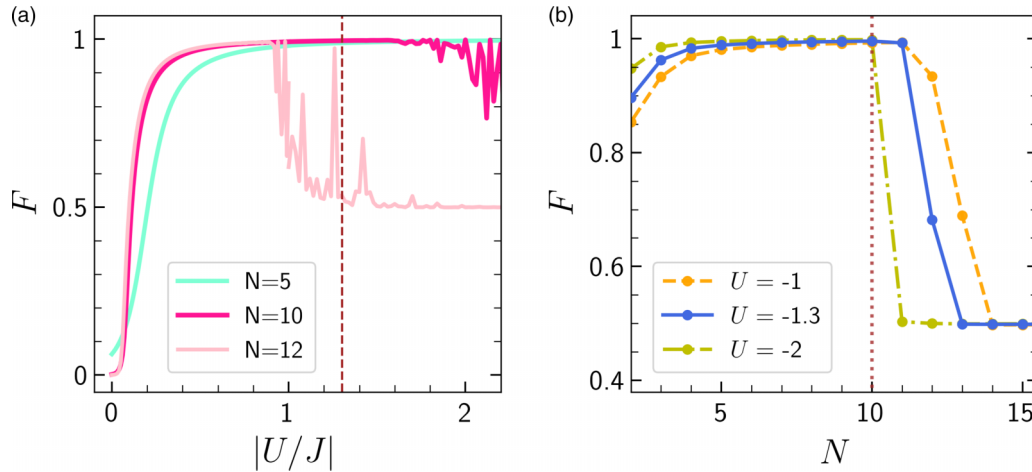


FIG. 11. (a) Fidelity vs $|U/J|$ for $U < 0$ and $N = 5$ (turquoise), $N = 10$ (magenta), and $N = 12$ (pink). (b) Fidelity vs N for $U = -1.0$ (dashed line), $U = -1.3$ (solid line), and $U = -2.0$ (dot dashed line). The vertical lines mark $|U/J| = 1.3$ and $N = 10$, values used in Sec. VII.

propagation theory [60] and is given by

$$\Delta\phi = \frac{\Delta(N_1 - N_3)}{|\partial_\phi \langle N_1 - N_3 \rangle|} = \frac{1}{\sqrt{N}},$$

where the notation $\Delta X = \sqrt{\langle X^2 \rangle - \langle X \rangle^2}$ is the standard deviation of operator X . The above result shows the uncertainty of parameter ϕ is the shot noise limited.

The sensitivity of parameter ϕ can be improved for the case of initial twin-Fock state $|n, 0, n\rangle$ at sites 1 and 3. This can be achieved by detecting the parity operator $\Pi_1 = e^{-i\pi N_1}$ [56], whose expectation value for the output state generated in Eq. (16) is given by

$$\langle \Pi_1 \rangle \equiv \langle \tilde{\Psi}_{\text{out}}(\phi) | \Pi_1 | \tilde{\Psi}_{\text{out}}(\phi) \rangle = P_n[\cos(2\phi - \pi)],$$

where

$$P_n(x) = \sum_{k=0}^{\lfloor n/2 \rfloor} \frac{(-1)^k}{2^n} \binom{n}{k} \binom{2n-2k}{n} x^{n-2k}$$

are the Legendre polynomials. The sensitivity of parameter ϕ can be estimated by

$$\Delta\phi = \frac{\Delta \Pi_1}{|\partial_\phi \langle \Pi_1 \rangle|}, \quad (\text{C1})$$

which shows the uncertainty of parameter ϕ approaches the Heisenberg limit $\Delta\phi \approx 1/(2n)$ when $\phi \approx \pi/2$ (see Ref. [56] for details).

-
- [1] C. E. Shannon, A mathematical theory of communication, *Bell Syst. Tech. J.* **27**, 379 (1948).
- [2] M. A. Nielsen and I. L. Chuang, Quantum computation and quantum information, *Phys. Today* **54**, 60 (2001).
- [3] J. Maldacena, S. H. Shenker, and D. Stanford, A bound on chaos, *J. High Energy Phys.* (2016) 106.
- [4] M. Fadel, T. Zibold, B. Décamps, and P. Treutlein, Spatial entanglement patterns and Einstein-Podolsky-Rosen steering in Bose-Einstein condensates, *Science* **360**, 409 (2018).
- [5] P. Imany, J. A. Jaramillo-Villegas, M. S. Alshaykh, J. M. Lukens, O. D. Odele, A. J. Moore, D. E. Leaird, M. Qi, and A. M. Weiner, High-dimensional optical quantum logic in large operational spaces, *npj Quantum Inf.* **5**, 59 (2019).
- [6] M. Niknam, L. F. Santos, and D. G. Cory, Sensitivity of quantum information to environment perturbations measured with a nonlocal out-of-time-order correlation function, *Phys. Rev. Res.* **2**, 013200 (2020).
- [7] G. Gordon and G. Rigolin, Generalized teleportation protocol, *Phys. Rev. A* **73**, 042309 (2006).
- [8] H. Häffner, C. Roos, and R. Blatt, Quantum computing with trapped ions, *Phys. Rep.* **469**, 155 (2008).
- [9] C. H. Bennett, G. Brassard, C. Crépeau, R. Jozsa, A. Peres, and W. K. Wootters, Teleporting an Unknown Quantum State via Dual Classical and Einstein-Podolsky-Rosen Channels, *Phys. Rev. Lett.* **70**, 1895 (1993).
- [10] X.-S. Ma, T. Herbst, T. Scheidl, D. Wang, S. Kropatschek, W. Naylor, B. Wittmann, A. Mech, J. Kofler, E. Anisimova *et al.*, Quantum teleportation over 143 kilometres using active feed-forward, *Nature (London)* **489**, 269 (2012).
- [11] M. Giustina, M. A. M. Versteegh, S. Wengerowsky, J. Handsteiner, A. Hochrainer, K. Phelan, F. Steinlechner, J. Kofler, J.-A. Larsson, C. Abellán, W. Amaya, V. Pruneri, M. W. Mitchell, J. Beyer, T. Gerrits, A. E. Lita, L. K. Shalm, S. W. Nam, T. Scheidl, R. Ursin *et al.*, Significant-Loophole-Free Test of Bell's Theorem with Entangled Photons, *Phys. Rev. Lett.* **115**, 250401 (2015).
- [12] W. Zhang, D.-S. Ding, Y.-B. Sheng, L. Zhou, B.-S. Shi, and G.-C. Guo, Quantum Secure Direct Communication with Quantum Memory, *Phys. Rev. Lett.* **118**, 220501 (2017).
- [13] Y.-B. Sheng, L. Zhou, and G.-L. Long, One-step quantum secure direct communication, *Sci. Bull.* **67**, 367 (2022).
- [14] L. Pezzè, A. Smerzi, M. K. Oberthaler, R. Schmied, and P. Treutlein, Quantum metrology with nonclassical states of atomic ensembles, *Rev. Mod. Phys.* **90**, 035005 (2018).
- [15] R. Kaubruegger, D. V. Vasilyev, M. Schulte, K. Hammerer, and P. Zoller, Quantum Variational Optimization of Ramsey Interferometry and Atomic Clocks, *Phys. Rev. X* **11**, 041045 (2021).
- [16] C. D. Marciniak, T. Feldker, I. Pogorelov, R. Kaubruegger, D. V. Vasilyev, R. van Bijnen, P. Schindler, P. Zoller, R. Blatt,

- and T. Monz, Optimal metrology with programmable quantum sensors, *Nature (London)* **603**, 604 (2022).
- [17] T. Fogarty, A. Kiely, S. Campbell, and T. Busch, Effect of interparticle interaction in a free-oscillation atomic interferometer, *Phys. Rev. A* **87**, 043630 (2013).
- [18] O. V. Marchukov, A. G. Volosniev, M. Valiente, D. Petrosyan, and N. T. Zinner, Quantum spin transistor with a Heisenberg spin chain, *Nat. Commun.* **7**, 13070 (2016).
- [19] T. Fogarty, L. Ruks, J. Li, and T. Busch, Fast control of interactions in an ultracold two atom system: Managing correlations and irreversibility, *SciPost Phys.* **6**, 021 (2019).
- [20] J. H. M. Jensen, J. J. Sørensen, K. Mølmer, and J. F. Sherson, Time-optimal control of collisional \sqrt{swap} gates in ultracold atomic systems, *Phys. Rev. A* **100**, 052314 (2019).
- [21] K. S. Christensen, S. E. Rasmussen, D. Petrosyan, and N. T. Zinner, Coherent router for quantum networks with superconducting qubits, *Phys. Rev. Res.* **2**, 013004 (2020).
- [22] D. S. Grün, L. H. Ymai, K. Wittmann W., A. P. Tonel, A. Foerster, and J. Links, Integrable Atomtronic Interferometry, *Phys. Rev. Lett.* **129**, 020401 (2022).
- [23] D. S. Grün, K. Wittmann W., L. H. Ymai, J. Links, and A. Foerster, Protocol designs for NOON states, *Commun. Phys.* **5**, 36 (2022).
- [24] R. Horodecki, P. Horodecki, M. Horodecki, and K. Horodecki, Quantum entanglement, *Rev. Mod. Phys.* **81**, 865 (2009).
- [25] I. Bloch, Ultracold quantum gases in optical lattices, *Nat. Phys.* **1**, 23 (2005).
- [26] R. Dumke, L. Amico, M. G. Boshier, K. Dieckmann, W. Li, T. C. Killian *et al.*, Roadmap on quantum optical systems, *J. Opt.* **18**, 093001 (2016).
- [27] S. I. Mistakidis, A. G. Volosniev, R. E. Barfknecht, T. Fogarty, T. Busch, A. Foerster, P. Schmelcher, and N. T. Zinner, Cold atoms in low dimensions—a laboratory for quantum dynamics, [arXiv:2202.11071](https://arxiv.org/abs/2202.11071) [cond-mat.quant-gas].
- [28] C. Trefzger, C. Menotti, B. Capogrosso-Sansone, and M. Lewenstein, Ultracold dipolar gases in optical lattices, *J. Phys. B: At., Mol. Opt. Phys.* **44**, 193001 (2011).
- [29] T. Lahaye, C. Menotti, L. Santos, M. Lewenstein, and T. Pfau, The physics of dipolar bosonic quantum gases, *Rep. Prog. Phys.* **72**, 126401 (2009).
- [30] D. Petter, G. Natale, R. M. W. van Bijnen, A. Patscheider, M. J. Mark, L. Chomaz, and F. Ferlaino, Probing the Roton Excitation Spectrum of a Stable Dipolar Bose Gas, *Phys. Rev. Lett.* **122**, 183401 (2019).
- [31] A. P. Tonel, L. H. Ymai, K. W. W., A. Foerster, and J. Links, Entangled states of dipolar bosons generated in a triple-well potential, *SciPost Phys. Core* **2**, 003 (2020).
- [32] K. W. Wilsmann, L. H. Ymai, A. P. Tonel, J. Links, and A. Foerster, Control of tunneling in an atomtronic switching device, *Commun. Phys.* **1**, 91 (2018).
- [33] L. Sá, P. Ribeiro, and T. Prosen, Integrable nonunitary open quantum circuits, *Phys. Rev. B* **103**, 115132 (2021).
- [34] Y. Miao and E. Vernier, Integrable Quantum Circuits from the Star-Triangle Relation, [arXiv:2302.12675](https://arxiv.org/abs/2302.12675) [cond-mat.stat-mech].
- [35] T. Villazon, A. Chandran, and P. W. Claeys, Integrability and dark states in an anisotropic central spin model, *Phys. Rev. Res.* **2**, 032052(R) (2020).
- [36] J. S. Van Dyke, G. S. Barron, N. J. Mayhall, E. Barnes, and S. E. Economou, Preparing Bethe ansatz eigenstates on a quantum computer, *PRX Quantum* **2**, 040329 (2021).
- [37] J. S. V. Dyke, E. Barnes, S. Economou, and R. I. Nepomechie, Preparing exact eigenstates of the open XXZ chain on a quantum computer, *J. Phys. A: Math. Theor.* **55**, 055301 (2021).
- [38] W. Li, M. Okyay, and R. I. Nepomechie, Bethe states on a quantum computer: Success probability and correlation functions, *J. Phys. A: Math. Theor.* **55**, 355305 (2022).
- [39] A. Sopena, M. H. Gordon, D. García-Martín, G. Sierra, and E. López, Algebraic Bethe circuits, *Quantum* **6**, 796 (2022).
- [40] NOON state, belonging to the class of Schrödinger cat states, is an “all and nothing” superposition of two different modes. See, for example, Refs. [23,60–63].
- [41] M. A. Baranov, Theoretical progress in many-body physics with ultracold dipolar gases, *Phys. Rep.* **464**, 71 (2008).
- [42] L. H. Ymai, A. P. Tonel, A. Foerster, and J. Links, Quantum integrable multi-well tunneling models, *J. Phys. A: Math. Theor.* **50**, 264001 (2017).
- [43] T. Lahaye, T. Pfau, and L. Santos, Mesoscopic Ensembles of Polar Bosons in Triple-Well Potentials, *Phys. Rev. Lett.* **104**, 170404 (2010).
- [44] G. J. Milburn, J. Corney, E. M. Wright, and D. F. Walls, Quantum dynamics of an atomic Bose-Einstein condensate in a double-well potential, *Phys. Rev. A* **55**, 4318 (1997).
- [45] E. R. Castro, J. Chávez-Carlos, I. Roditi, L. F. Santos, and J. G. Hirsch, Quantum-classical correspondence of a system of interacting bosons in a triple-well potential, *Quantum* **5**, 563 (2021).
- [46] K. Wittmann W., E. R. Castro, A. Foerster, and L. F. Santos, Interacting bosons in a triple well: Preface of many-body quantum chaos, *Phys. Rev. E* **105**, 034204 (2022).
- [47] R. Islam, R. Ma, P. M. Preiss, M. Eric Tai, A. Lukin, M. Rispoli, and M. Greiner, Measuring entanglement entropy in a quantum many-body system, *Nature (London)* **528**, 77 (2015).
- [48] J. G. Rarity, P. R. Tapster, E. Jakeman, T. Larchuk, R. A. Campos, M. C. Teich, and B. E. A. Saleh, Two-Photon Interference in a Mach-Zehnder Interferometer, *Phys. Rev. Lett.* **65**, 1348 (1990).
- [49] R. Lewis-Swan and K. Kheruntsyan, Proposal for demonstrating the Hong-Ou-Mandel effect with matter waves, *Nat. Commun.* **5**, 3752 (2014).
- [50] B. Yurke, S. L. McCall, and J. R. Klauder, SU(2) and SU(1,1) interferometers, *Phys. Rev. A* **33**, 4033 (1986).
- [51] T. Berrada, S. Van Frank, R. Bücker, T. Schumm, J.-F. Schaff, and J. Schmiedmayer, Integrated Mach-Zehnder interferometer for Bose-Einstein condensates, *Nat. Commun.* **4**, 2077 (2013).
- [52] S. Bose, V. Vedral, and P. L. Knight, Multiparticle generalization of entanglement swapping, *Phys. Rev. A* **57**, 822 (1998).
- [53] J. A. Dunningham, S. Bose, L. Henderson, V. Vedral, and K. Burnett, Entanglement concentration in Bose-Einstein condensates, *Phys. Rev. A* **65**, 064302 (2002).
- [54] L. Zhou, Y.-B. Sheng, W.-W. Cheng, L.-Y. Gong, and S.-M. Zhao, Efficient entanglement concentration for arbitrary less-entangled NOON states, *Quantum Inf. Process.* **12**, 1307 (2013).
- [55] M. M. Cunha, A. Fonseca, and E. O. Silva, Tripartite entanglement: Foundations and applications, *Universe* **5**, 209 (2019).
- [56] R. J. Birrell, P. M. Alsing, and C. C. Gerry, The parity

- operator: Applications in quantum metrology, [AVS Quantum Sci. **3**, 014701 \(2021\)](#).
- [57] T. Koch, T. Lahaye, J. Metz, B. Fröhlich, A. Griesmaier, and T. Pfau, Stabilization of a purely dipolar quantum gas against collapse, [Nat. Phys. **4**, 218 \(2008\)](#).
- [58] J. Links, A. Foerster, A. P. Tonel, and G. Santos, The two-site Bose–Hubbard model, in *Ann. Henri Poincaré*, (Springer, New York, 2006), Vol. 7, pp. 1591–1600.
- [59] A. A. Bychek, D. N. Maksimov, and A. R. Kolovsky, Noon state of Bose atoms in the double-well potential via an excited-state quantum phase transition, [Phys. Rev. A **97**, 063624 \(2018\)](#).
- [60] H. Lee, P. Kok, and J. P. Dowling, A quantum Rosetta stone for interferometry, [J. Mod. Opt. **49**, 2325 \(2002\)](#).
- [61] I. Afek, O. Ambar, and Y. Silberberg, High-NOON states by mixing quantum and classical light, [Science **328**, 879 \(2010\)](#).
- [62] S.-F. Qi and J. Jing, Generating entangled states from coherent states in circuit QED, [Phys. Rev. A **107**, 042412 \(2023\)](#).
- [63] S.-F. Qi and J. Jing, Floquet generation of a magnonic NOON state, [Phys. Rev. A **107**, 013702 \(2023\)](#).